



# Active contours driven by local pre-fitting energy for fast image segmentation

Keyan Ding<sup>a</sup>, Linfang Xiao<sup>b</sup>, Guirong Weng<sup>a,\*</sup>

<sup>a</sup>School of Mechanical and Electric Engineering, Soochow University, Suzhou 215021, China

<sup>b</sup>College of Biosystems Engineering and Food Science, Zhejiang University, Hangzhou 310058, China

## ARTICLE INFO

### Article history:

Received 25 August 2017

### Keywords:

Image segmentation  
Active contour model  
Level set method  
Robust initialization  
Local pre-fitting

## ABSTRACT

Local fitting-based active contour models can segment images with intensity inhomogeneity effectively, but they are time-consuming and often fall into local minima. In this paper, we present an active contour model using local pre-fitting energy for fast image segmentation. The core idea of local pre-fitting energy is to define two pre-fitting functions by computing average image intensities locally before the evolution of curve. Experiments have shown that the proposed model is robust to initialization, which allows the initial level set function to be a small constant function. And it costs less segmentation time compared to other local fitting-based models. In addition, the proposed local pre-fitting method can be applied to other local fitting-based models to improve the robustness of initial contours and reduce the computational costs.

© 2018 Elsevier B.V. All rights reserved.

## 1. Introduction

Image segmentation is a fundamental problem in the field of image processing and computer vision. Over the past decades, many famous image segmentation methods have been presented, such as region grow, watershed algorithm and graph cut [1,2]. Active contour models have been widely applied in image segmentation since the presentation by Kass et al. [3]. Existing active contour models can be roughly categorized into two basic classes: edge-based models [4–11] and region-based models [12–27,29]. Edge-based models often use an edge indicator to drive the curve towards the object boundaries, such as GAC model [4,5]. Region-based models often use a certain region descriptor to find a partition on the image domain. Chan–Vese (CV) model [13] is a well-known region-based model and has been widely used in practice applications. But the CV model cannot work well for images with intensity inhomogeneity due to the assumption that the image intensities are statistically homogeneous. To handle the intensity inhomogeneity which is often occurred in medical and natural images, Chan and Vese [14] proposed a piecewise smooth (PS) model. It has exhibited certain capability of segmenting images with intensity inhomogeneity. However, the computational efficiency is much low.

Li et al. [16] presented an active contour model based on region-scalable fitting (RSF) energy. The RSF model draws upon the

local image information by a kernel function. With the information of local image intensities, the RSF model can effectively segment images with intensity inhomogeneity. But when the initial contour is set inappropriately, the RSF model will be stuck in local minima because the energy functional is non-convex [28,29]. In addition, the time cost is relatively large due to the computation of four convolutions in each iteration. Zhang et al. [18] presented an active contour model driven by local image fitting (LIF) energy. By extracting the local image information, it is able to segment images with intensity inhomogeneity. Compared to the RSF model, the computational cost of LIF model is smaller because only two convolutions are computed in each iteration. However, the problem of initial contours has not been solved. Liu et al. [19] proposed a local region-based Chan–Vese (LRCV) model. Similarly, it can segment images with intensity inhomogeneity, and the computational cost is lower than the RSF model. But it is sensitive to initial contours. Wang et al. [20] presented an active contour model based on local Gaussian distribution fitting (LGDF) energy. It defines a local Gaussian distribution fitting energy by using local means and variances as variables. The LGDF model is able to distinguish regions with similar intensity means but different variances. But the problem of initialization is still unsolved and the segmentation speed is low due to the extra computation of variances. Considering that the object and background in many real-world images are hard to be described by a predefined distribution, Liu et al. [21] proposed a nonparametric active contour model driven by the local histogram fitting (LHF) energy. It defines two fitting histograms that approximate the distribution of object and background locally. The

\* Corresponding author.

E-mail address: [wgr@suda.edu.cn](mailto:wgr@suda.edu.cn) (G. Weng).

LHF model can segment the regions whose distribution is hard to be predefined. However, it has much high computational costs because the histogram distribution of each grey value needs to be calculated. Likewise, it is sensitive to initialization.

In summary, active contour models based on local information fitting energy [16–24] can segment images with intensity inhomogeneity effectively. However, an inappropriate initial contour will cause a wrong segmentation. Moreover, the segmentation cost of these models is high in general.

In this paper, we present an active contour model driven by local pre-fitting energy for image segmentation, which is robust to initialization and has low computational costs. First, we define two pre-fitting functions by computing average image intensities locally before the evolution of curve. Next, an energy based on local pre-fitting functions is proposed, and then incorporated into the variational level set formulation with a length constraint term and a distance regularized term. The steepest descent method is used to minimize the energy functional. Experiments have shown that the proposed model can efficiently segment images with intensity inhomogeneity. As an application, the proposed model can be used for denoising and improving image contrast. In addition, the proposed local pre-fitting method can be easily applied to other local region fitting-based models to improve the segmentation speed and the robustness against initialization.

The remainder of this paper is organized as follows. Section 2 briefly reviews some well-known local fitting-based models, including the RSF model [16], the LIF model [18] and the LGDF model [20]. Section 3 introduces our model using local pre-fitting energy. Section 4 shows some experimental results of the proposed model. Section 5 presents some discussions. Last, Section 6 concludes this paper.

## 2. The related works

### 2.1. Region-scalable fitting model

Li et al. [16,17] proposed a region-scalable fitting (RSF) model for segmenting images with intensity inhomogeneity. They define the following energy functional:

$$\begin{aligned} E^{RSF}(\phi, f_1, f_2) = & \lambda_1 \int_{\Omega} \left( \int_{\Omega} K_{\sigma}(x-y) |I(y) - f_1(x)|^2 H_{\varepsilon}(\phi(y)) dy \right) dx \\ & + \lambda_2 \int_{\Omega} \left( \int_{\Omega} K_{\sigma}(x-y) |I(y) - f_2(x)|^2 [1 - H_{\varepsilon}(\phi(y))] dy \right) dx \\ & + \nu \int_{\Omega} \delta_{\varepsilon}(\phi(x)) |\nabla \phi(x)| dx + \mu \int_{\Omega} \frac{1}{2} (|\nabla \phi(x)| - 1)^2 dx \end{aligned} \quad (1)$$

where,  $x, y \in \Omega$ ,  $\lambda_1, \lambda_2, \nu$  and  $\mu$  are positive constants.  $K_{\sigma}$  is a Gaussian kernel function with standard deviation  $\sigma$ .  $f_1(x)$  and  $f_2(x)$  are two smooth functions that approximate the intensities of image outside and inside the contour  $C$  in a local region, respectively.  $H_{\varepsilon}(x)$  and  $\delta_{\varepsilon}(x)$  are regularized Heaviside and Dirac function defined by

$$\begin{cases} H_{\varepsilon}(x) = \frac{1}{2} \left( 1 + \frac{2}{\pi} \arctan \left( \frac{x}{\varepsilon} \right) \right) \\ \delta_{\varepsilon}(x) = \frac{\varepsilon}{\pi(\varepsilon^2 + x^2)} \end{cases} \quad (2)$$

The method of steepest descent is used to minimize the energy functional (1). Keeping level set function  $\phi$  fixed and minimizing  $E^{RSF}$  with respect to  $f_1$  and  $f_2$ , the following formulations can be obtained:

$$\begin{cases} f_1(x) = \frac{\int_{\Omega} K_{\sigma}(x-y) [H_{\varepsilon}(\phi(y)) \cdot I(y)] dy}{\int_{\Omega} K_{\sigma}(x-y) H_{\varepsilon}(\phi(y)) dy} \\ f_2(x) = \frac{\int_{\Omega} K_{\sigma}(x-y) [(1 - H_{\varepsilon}(\phi(y))) \cdot I(y)] dy}{\int_{\Omega} K_{\sigma}(x-y) [1 - H_{\varepsilon}(\phi(y))] dy} \end{cases} \quad (3)$$

Keeping  $f_1$  and  $f_2$  fixed and minimizing  $E^{RSF}$  with respect to the level set function  $\phi$ , the following gradient descent flow can be

obtained:

$$\begin{aligned} \frac{\partial \phi}{\partial t} = & -\delta_{\varepsilon}(\phi) (\lambda_1 e_1 - \lambda_2 e_2) + \nu \delta_{\varepsilon}(\phi) \operatorname{div} \left( \frac{\nabla \phi}{|\nabla \phi|} \right) \\ & + \mu \left( \nabla^2 \phi - \operatorname{div} \left( \frac{\nabla \phi}{|\nabla \phi|} \right) \right) \end{aligned} \quad (4)$$

where  $e_1$  and  $e_2$  are

$$\begin{cases} e_1(x) = \int_{\Omega} K_{\sigma}(y-x) |I(x) - f_1(y)|^2 dy \\ e_2(x) = \int_{\Omega} K_{\sigma}(y-x) |I(x) - f_2(y)|^2 dy \end{cases} \quad (5)$$

### 2.2. Local image fitting model

Zhang et al. [18] presented an active contour model driven by local image fitting (LIF) energy. This energy functional is defined by minimizing the difference between the fitted image and the original image:

$$E^{LIF}(\phi, m_1, m_2) = \frac{1}{2} \int_{\Omega} |I(x) - I^{fit}(x)|^2 dx \quad (6)$$

where  $I^{fit}$  is the local fitting image defined as follows:

$$I^{fit}(x) = m_1(x) H_{\varepsilon}(\phi(x)) + m_2(x) [1 - H_{\varepsilon}(\phi(x))] \quad (7)$$

with

$$\begin{cases} m_1(x) = \operatorname{mean}(I(x) : x \in \{\phi(x) < 0\} \cap \Omega_w(x)) \\ m_2(x) = \operatorname{mean}(I(x) : x \in \{\phi(x) > 0\} \cap \Omega_w(x)) \end{cases} \quad (8)$$

where  $m_1(x)$  and  $m_2(x)$  can be seen as the weighted averages of the image intensities in a Gaussian window  $\Omega_w$  outside and inside the contour, respectively. Thus,  $m_1(x)$  and  $m_2(x)$  are totally the same to  $f_1(x)$  and  $f_2(x)$  in the RSF model. Similarly, the steepest descent method is used to minimize the energy functional (6). By introducing the local image information, the LIF model is able to segment images with intensity inhomogeneity and the computational cost is lower because only two convolutions are computed in each iteration, which is about half of that in the RSF model. However, it is sensitive to initialization, like the RSF model.

### 2.3. Local Gaussian distribution fitting model

Wang et al. [20] presented an active contour model based on local Gaussian distribution fitting (LGDF) energy. It defines a local Gaussian distribution fitting energy by using local means and variances as variables:

$$\begin{aligned} E^{LGDF}(\phi, p_{1,x}, p_{2,x}) = & \int_{\Omega} \left( \int_{\Omega} K_{\sigma}(x-y) \log p_{1,x}(I(y)) H_{\varepsilon}(\phi(y)) dy \right) dx \\ & + \int_{\Omega} \left( \int_{\Omega} K_{\sigma}(x-y) \log p_{2,x}(I(y)) [1 - H_{\varepsilon}(\phi(y))] dy \right) dx \end{aligned} \quad (9)$$

where  $P_{1,x}$  and  $P_{2,x}$  are

$$p_{i,x}(I(y)) = \frac{1}{\sqrt{2\pi} \sigma_i(x)} \exp \left( -\frac{u_i(x) - I(y)}{2\sigma_i^2(x)} \right), i = 1, 2 \quad (10)$$

where  $u_1(x)$  and  $u_2(x)$  can be seen as the weighted averages of the image intensities in a Gaussian window outside and inside the contour, respectively.  $\sigma_1^2(x)$  and  $\sigma_2^2(x)$  can be seen as the weighted variances of the image intensities in a Gaussian window outside and inside the contour, respectively. Note,  $u_1(x)$  and  $u_2(x)$  are also the same to  $f_1(x)$  and  $f_2(x)$  in the RSF model, and the LGDF model will be the same as the RSF model if  $\sigma_i^2(x) = 0.5$ . By computing both the first order and second order statistics of local intensity information, the LGDF model can better handle intensity inhomogeneity and noise, and differentiate regions with similar intensity means but different intensity variances. But the problem of initialization is still unsolved and the computational cost is large due to the extra computation of variances.

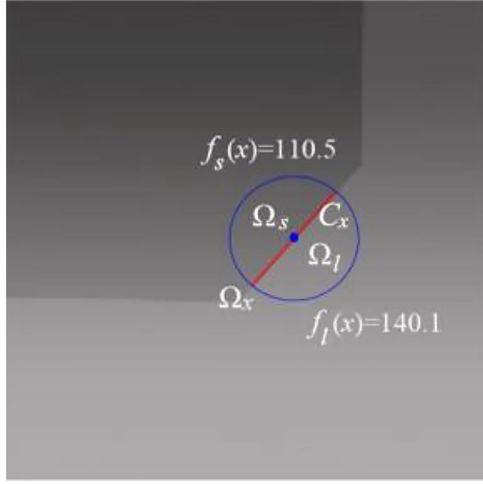


**Fig. 1.** Illustration of the region  $\Omega_x$ ,  $\Omega_s$  and  $\Omega_l$ , and the values of  $f_s(x)$  and  $f_l(x)$  on an edge point  $x$ . The blue line represents the region  $\Omega_x$  with center point  $x$ . The red line  $C_x$  represents the boundary of  $\Omega_s$  and  $\Omega_l$ . (For interpretation of the references to colour in this figure legend, the reader is referred to the web version of this article.)

### 3. The proposed method

In this section, we will present an active contour model using local pre-fitting energy. Let  $\Omega \subset \mathbb{R}^2$  be the image domain, and  $I(x): \Omega \rightarrow \mathbb{R}$  be a given gray image. We define the following functions:

$$\begin{cases} f_m(x) = \text{mean}(I(y) | y \in \Omega_x) \\ f_s(x) = \text{mean}(I(y) | y \in \Omega_s) \\ f_l(x) = \text{mean}(I(y) | y \in \Omega_l) \end{cases} \quad (11)$$

where  $\Omega_x$  represents a small neighborhood centered at  $x$  with radius  $w$ .  $\Omega_s$  and  $\Omega_l$  are defined by

$$\begin{cases} \Omega_s = \{y | I(y) < f_m(x)\} \cap \Omega_x \\ \Omega_l = \{y | I(y) > f_m(x)\} \cap \Omega_x \end{cases} \quad (12)$$

It means  $\Omega_s$  is the region where the image intensities smaller than the average intensities in  $\Omega_x$ , and  $\Omega_l$  is the region where the image intensities larger than the average intensities in  $\Omega_x$ .  $f_m(x)$ ,  $f_s(x)$  and  $f_l(x)$  are the average intensities in  $\Omega_x$ ,  $\Omega_s$  and  $\Omega_l$ , respectively.

According to Eqs. (11) and (12), for a given  $\Omega_x$ , the functions  $f_s(x)$  and  $f_l(x)$  can be calculated directly. For instance, Fig. 1 shows the region  $\Omega_x$ ,  $\Omega_s$ ,  $\Omega_l$  and dividing line  $C_x$ , and the values of  $f_s(x)$  and  $f_l(x)$  on an edge point  $x$ .

Next, we propose the following local energy function:

$$E_x(C) = \int_{\text{outside}(C) \cap \Omega_x} |I(y) - f_s(x)|^2 dy + \int_{\text{inside}(C) \cap \Omega_x} |I(y) - f_l(x)|^2 dy \quad (13)$$

Given a center point  $x$ , the above energy can be minimized when the contour  $C$  is exactly on the object boundary, like the red line  $C_x$  in Fig. 1.

The Gaussian kernel function  $K_\sigma$ , which is often used in local fitting-based models due to its localization property, can be used to replace the local window  $\Omega_x$ . Thus,  $E_x$  in Eq. (13) can be rewritten as

$$E_x(C) = \int_{\text{outside}(C)} K_\sigma(x-y) |I(y) - f_s(x)|^2 dy + \int_{\text{inside}(C)} K_\sigma(x-y) |I(y) - f_l(x)|^2 dy \quad (14)$$

For all the points  $x$  in the image domain  $\Omega$ , we need to minimize the integral of  $E_x$ . Thus, we propose the following energy functional  $E^{LPF}$ :

$$E^{LPF}(C) = \int_{\Omega} \left( \int_{\text{outside}(C)} K_\sigma(x-y) |I(y) - f_s(x)|^2 dy \right) dx + \int_{\Omega} \left( \int_{\text{inside}(C)} K_\sigma(x-y) |I(y) - f_l(x)|^2 dy \right) dx \quad (15)$$

When  $E^{LPF}$  is minimized, the curve  $C$  will contain the curves located on the boundaries. But there will be some excess curves on the region far away the boundaries. Therefore, it is necessary to add the length constraint term  $L(\phi)$  for smoothing and shortening the curve, which is used in most active contour models [16]. Besides, we add the distance regularized term  $P(\phi)$  for free of reinitialization [9].

Using the zero level set of a Lipschitz function  $\phi$  to represent the curve  $C$ , the entire energy functional can be expressed as

$$\mathcal{F}^{LPF}(\phi) = E^{LPF}(\phi) + \nu L(\phi) + \mu P(\phi) \quad (16)$$

where  $\nu$  and  $\mu$  are the coefficient of length term and distance regularized term, respectively.  $E^{LPF}(\phi)$ ,  $L(\phi)$  and  $P(\phi)$  are defined by

$$E^{LPF}(\phi) = \int_{\Omega} \left( \int_{\Omega} K_\sigma(x-y) |I(y) - f_s(x)|^2 H_\varepsilon(\phi(y)) dy \right) dx + \int_{\Omega} \left( \int_{\Omega} K_\sigma(x-y) |I(y) - f_l(x)|^2 (1 - H_\varepsilon(\phi(y))) dy \right) dx \quad (17)$$

$$L(\phi) = \int_{\Omega} \delta(\phi) |\nabla \phi(x)| dx \quad (18)$$

$$P(\phi) = \int_{\Omega} \frac{1}{2} (|\nabla \phi(x)| - 1)^2 dx \quad (19)$$

Using the steepest descent method to minimize the energy functional (16) with respect to the level set function  $\phi$ , we can obtain the following gradient descent flow:

$$\begin{aligned} \frac{\partial \phi}{\partial t} = & -\delta_\varepsilon(\phi) (e_s(x) - e_l(x)) + \nu \delta_\varepsilon(\phi) \text{div} \left( \frac{\nabla \phi}{|\nabla \phi|} \right) \\ & + \mu \left( \nabla^2 \phi - \text{div} \left( \frac{\nabla \phi}{|\nabla \phi|} \right) \right) \end{aligned} \quad (20)$$

where  $e_s(x)$  and  $e_l(x)$  are

$$\begin{cases} e_s(x) = \int_{\Omega} K_\sigma(y-x) |I(y) - f_s(x)|^2 dy \\ e_l(x) = \int_{\Omega} K_\sigma(y-x) |I(y) - f_l(x)|^2 dy \end{cases} \quad (21)$$

where  $f_s(x)$  and  $f_l(x)$  are computed according to Eqs. (11) and (12). In the proposed model,  $f_s(x)$  and  $f_l(x)$  can be seen as the fitting functions that locally approximate the image intensities on the two sides of the curve  $C$ . Because the fitting functions  $f_s(x)$  and  $f_l(x)$  are computed before curve evolution and do not need to be updated in each iteration, we term  $f_s(x)$  and  $f_l(x)$  as local pre-fitting (LPF) functions, and the corresponding energy is termed as LPF energy. In traditional local fitting-based model, such as the RSF model,  $f_1(x)$  and  $f_2(x)$  need to be updated in each iteration with the change of level set function  $\phi$ , and the computation cost is large. In the proposed model, the pre-fitting functions  $f_s(x)$  and  $f_l(x)$  have nothing to do with the level set function  $\phi$ . They are calculated only once at the beginning of the evolution and do not need to be updated in each iteration. Therefore, the proposed model has lower computational costs than traditional local fitting-based model.



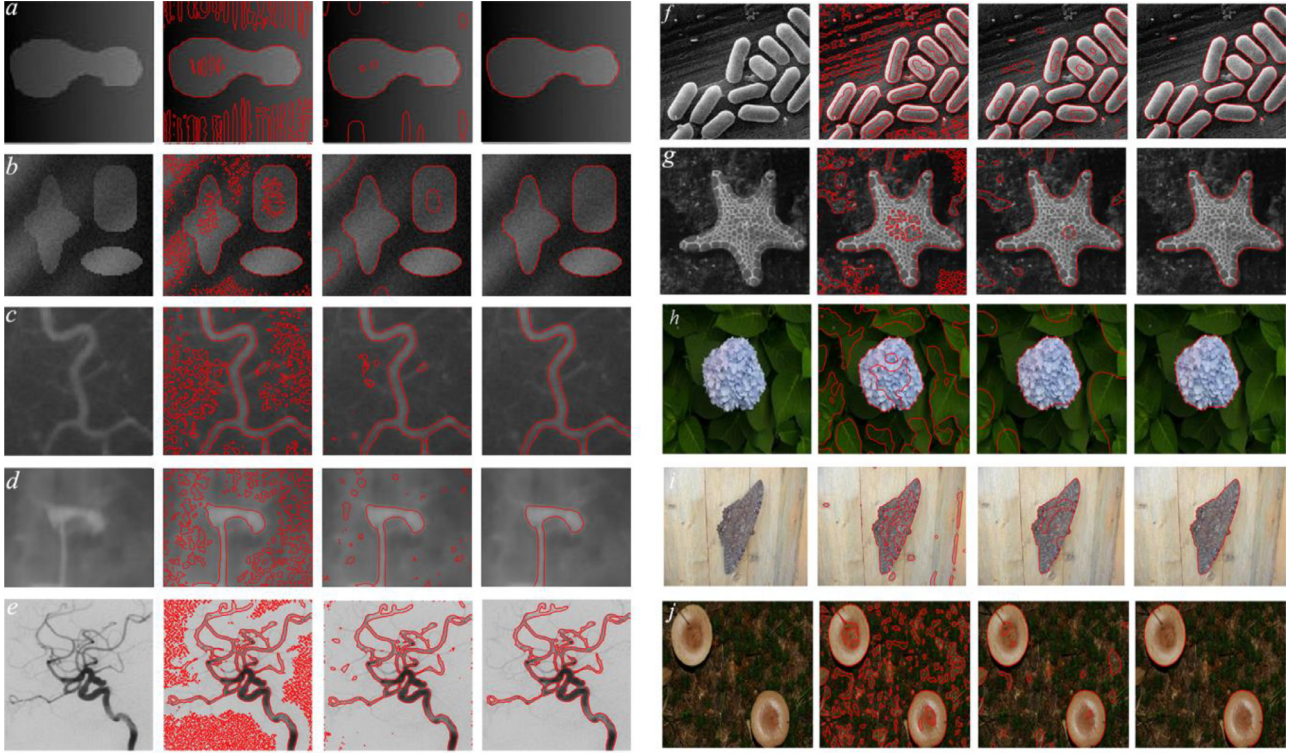


**Fig. 2.** Segmentation results of the proposed method for some images. First column: original image. Second and third columns: intermediate segmentation results. Last column: final segmentation results.

## 4. Implementation and experimental results

### 4.1. Implementation

In this section, the proposed model using local pre-fitting energy will be tested by segmentating some synthetic and real images, and the results will be compared with some well-known local fitting-based models. The implementation of our model is presented below:

Step 1. Set various parameters, including the initial level set function  $\phi_0$ .

Step 2. Compute  $f_s(x)$  and  $f_l(x)$  according to Eqs. (11) and (12).

Step 3. Go to the next point  $x = x + 1$ , and return to Step 2 until all points are computed.

Step 4. Update the level set function  $\phi$  according to Eqs. (20) and (21) until the convergence criterion is reached.

Note that the implementation of pre-fitting operation (Step 2 and Step 3) is straightforward and fast because it scans the image only once. In the procedure of calculating Eq. (20), the spatial partial derivatives  $\partial\phi/\partial x$  and  $\partial\phi/\partial y$  are discretized as central difference and the temporal partial derivative  $\partial\phi/\partial t$  is discretized as forward difference. Thus, Eq. (20) can be written as

$$\phi_{i,j}^{k+1} = \phi_{i,j}^k + \Delta t \times R(\phi_{i,j}^k) \quad (22)$$

where  $\Delta t$  is the time step, and  $R(\phi_{i,j}^k)$  is the approximation of the right-hand side in Eq. (20).

In the proposed model, the initial level set function  $\phi_0$  is set to a small constant function  $\phi_0(x) = c_0$ . The stopping criteria of curve evolution is  $|(S_{i+5} - S_i)/S| < 10^{-5}$ .  $S$  represents the total area of image.  $S_i$  represents the area surrounded by the contour at the time  $i$ . Unless otherwise specified, we use the following parameters in this paper:  $c_0 = 1$ ,  $\mu = 2$ ,  $\nu = 0.02 \times 255^2$ ,  $\varepsilon = 1$  and  $\Delta t = 0.1$ , the size of  $K_\sigma$  is  $w = 13 \times 13$  and the standard deviation  $\sigma = 3$ .

**Table 1**

The values of parameters used in Fig. 2.

Image	The length term $\nu$	The size of local window $w \times w$
a	$0.03 \times 255^2$	$13 \times 13$
b	$0.02 \times 255^2$	$13 \times 13$
c	$0.02 \times 255^2$	$13 \times 13$
d	$0.03 \times 255^2$	$13 \times 13$
e	$0.005 \times 255^2$	$13 \times 13$
f	$0.1 \times 255^2$	$13 \times 13$
g	$0.2 \times 255^2$	$17 \times 17$
h	$0.5 \times 255^2$	$17 \times 17$
i	$0.1 \times 255^2$	$13 \times 13$
j	$0.1 \times 255^2$	$13 \times 13$

### 4.2. Segmentation results of proposed model

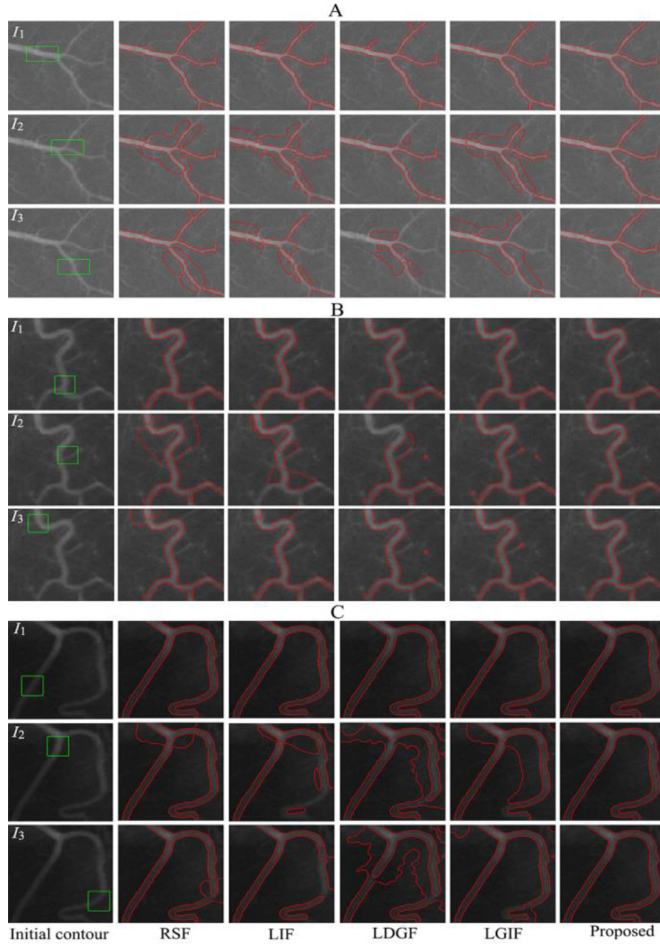
Fig. 2 shows the segmentation results of the proposed model for some synthetic and real images. These images have typical intensity inhomogeneity, weak edges, low contrast or noises, and the last three images are color images. Fig. 2 shows that the satisfactory segmentation results for these images have been obtained by using the proposed model. (The values of some parameters are shown in Table 1, unlisted parameters are defaults).

### 4.3. Comparisons with some region-based models

This section compares the results of the proposed model with some well-known region-based models, including the RSF model [16], the LIF model [18], the LGDF model [20] and the LGIF model [26]. Take three vessel images in Fig. 3 for examples, we set three different initial contours in each image. Each initial level set function  $\phi_0$  is initialized as a binary step function which takes  $-c_0$  inside zero level set and  $c_0$  outside. The parameters used in the RSF model are  $c_0 = 2$ ,  $\sigma = 3$ ,  $\varepsilon = 1$ ,  $\lambda_1 = 1$ ,  $\lambda_2 = 1$ ,  $u = 1$ ,

**Table 2**The number of iterations, the time spent and the DSC of the images A, B and C under the initial contour  $I_1$ .

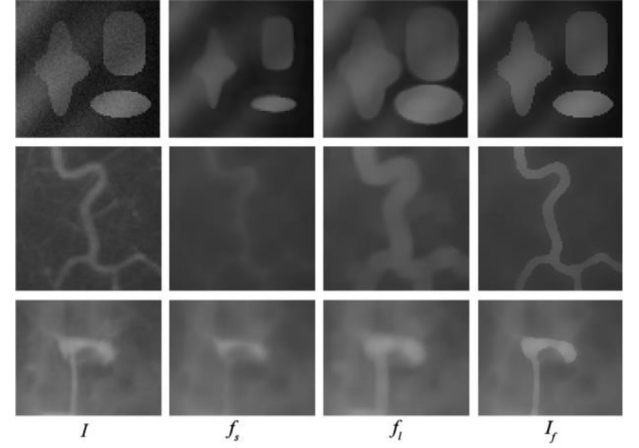
Models	Image A (168 × 156) Iterations/Time(s)/DSC	Image B (111 × 110) Iterations/Time(s)/DSC	Image C (103 × 105) Iterations/Time(s)/DSC
RSF	182/1.442/0.9131	105/0.648/0.9833	236/1.458/0.9509
LIF	322/1.976/0.8905	274/1.180/0.9821	405/1.742/0.9237
LGDF	305/3.856/0.8916	405/3.682/0.9636	550/4.637/0.9430
LGIF	130/1.201/0.9533	152/1.048/0.9701	55/0.374/0.9441
Our	54/0.338/0.9524	32/0.162/0.9818	20/0.128/0.9711

**Fig. 3.** Comparisons on the segmentation results of the RSF model, the LIF model, the LGDF model, the LGIF model and the proposed model with different initial contours for three vessel images.

$v = 0.001 \times 255^2$  and  $\Delta t = 0.1$ . In the LIF model,  $c_0 = 2$ ,  $\sigma = 3$ ,  $\varepsilon = 1$ ,  $\Delta t = 0.05$ , the size of regularized Gaussian kernel is  $5 \times 5$ , and its variance is 0.5. In the LGDF model,  $c_0 = 2$ ,  $\sigma = 3$ ,  $\varepsilon = 1$ ,  $\lambda_1 = 1$ ,  $\lambda_2 = 1$ ,  $u = 1$ ,  $v = 0.0001 \times 255^2$  and  $\Delta t = 0.1$ . In the LGIF model,  $c_0 = 2$ ,  $\sigma = 3$ ,  $\varepsilon = 1$ ,  $\lambda_1 = 1$ ,  $\lambda_2 = 1$ ,  $w = 0.05$ ,  $u = 1$ ,  $v = 0.001 \times 255^2$  and  $\Delta t = 0.1$ . All of the models are implemented in Matlab R2012b on an Inter(R) Core(TM) i5-6500 3.2 GHz personal computer.

From Fig. 3, we notice that the segmentation results using the initial contour  $I_1$  in the RSF, LIF, LGDF and LGIF models are satisfactory, but the results using the initial contours  $I_2$  and  $I_3$  are undesired. In the proposed model, the desired segmentation results can be obtained under each initial contour. These three experiments demonstrate that the change of initial contours has no influence on the segmentation results in the proposed model. That means our model is more robust to initial contours.

Table 2 shows the number of iterations, the time spent and the dice similarity coefficient (DSC) of the images A, B and C in Fig. 3.

**Fig. 4.** Results of the fitting image for three different images.

DSC is defined by

$$DSC = \frac{2(S_1 \cap S_2)}{S_1 + S_2} \quad (23)$$

where  $S_1$  represents the ground-truth region and  $S_2$  represents the region solved by the model. Note, we only list these quantitative results under the initial contour  $I_1$ , and the results of ground-truth are obtained by manually.

From Table 2, we conclude that both the number of iterations and the time spent of our model are the least in these models. The LGDF model has the longest segmentation time and the largest number of iterations because of the extra computation of image variances in each iteration. The LIF model also needs a large number of iterations, but its segmentation time is relatively short due to the low computation cost in each iteration. The RSF model needs less segmentation time and fewer number of iterations than the LIF model and the LGDF model for these images. In the LGIF model, the segmentation time is influenced by the weight between local and global energy. For the image C, the time spent is very short due to a suitable weight  $w$ . But for the image A and B, the segmentation time is relatively long under this weight  $w$ . In the proposed model, both the number of iterations and segmentation time are much less than above models. It proves that using the local pre-fitting method is conducive to achieve fast segmentation.

#### 4.4. Application of the proposed model

The proposed model can be applied for reducing the noise and improving image contrast. We defines the following fitting image  $I_f$ :

$$I_f = f_s \cdot H_\varepsilon(\phi_n) + f_i \cdot [1 - H_\varepsilon(\phi_n)] \quad (24)$$

where  $\phi_n$  is the final level set function.

Fig. 4 shows the original image  $I$ , the image  $f_s$ , the image  $f_i$  and the fitting image  $I_f$  for some images in Fig. 2. By comparing the left-most column with the right-most column of Fig. 4, we discover that the fitting image has reduced the noise and the object



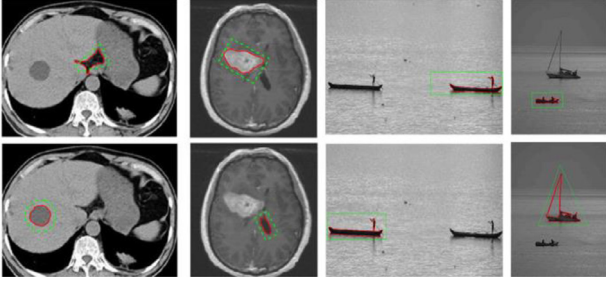


**Fig. 5.** Segmentations of specific local region. The selected rough region of objects and the final segmentation results are plotted as the green dotted line and solid red line, respectively. (For interpretation of the references to colour in this figure legend, the reader is referred to the web version of this article.)

became brighter and the background became darker. Moreover, the boundaries of objects are enhanced significantly.

## 5. Discussions

### 5.1. Initialization of level set function

In the proposed model, the initial level set function  $\phi_0$  is set to be a small constant function. According to the definition of Dirac function  $\delta_\varepsilon$  in Eq. (2), we can know that  $\delta_\varepsilon(x)$  is not strictly equal to zero on the nonzero points. According to Eq. (21), for points near the boundaries, the values of  $(e_l(x) - e_s(x))$  is very large. Therefore, although  $\delta_\varepsilon(\phi_0)$  takes small values far from the zero level set, the value of  $-\delta_\varepsilon(\phi_0)(e_l(x) - e_s(x))$  is still large near the boundaries, which can change the value of level set function  $\phi$ . Thus, new zero level contours will be emerged quickly at the boundaries after several iterations. Note, a larger value of  $\varepsilon$  or a smaller value of  $c$  makes  $\delta_\varepsilon(\phi_0)$  larger so that new contours are more likely to emerge. In addition, the regularization term  $P(\phi)$  in Eq. (19) can inherently guarantee the regularity of the level set function  $\phi$  in the process of curve evolution [9]. Therefore, setting  $\phi_0$  as a small constant function in the proposed model is feasible, and the segmentation result can be obtained more easily.

### 5.2. Segmentation of specific local region

In last Section, we have explained the reason about the fast emergence of new contours at the object boundaries. However, because new contours are emerged too fast even at the regions far away the initial contour, the proposed model often segments the whole image. Thus, it is difficult to detect a single target from a complex background, such as local lesions in medical computed tomography (CT) images. Here we provide a simple scheme to segment a specific local region. We can interactively select a rough region contained the target and use pre-fitting operations only to this region. Thus, only in this region exists the fitting energy to drive the evolution of curve and other regions will not appear curves. In this way, the proposed model can achieve local segmentation.

Fig. 5 shows two medical images and two ship images with multiple objects. A rough region is selected interactively, as plotted in the green dotted line of Fig. 5. And the corresponding segmentation results are plotted by the red line. Fig. 5 demonstrates that the proposed model can accurately detect the specific targets, such as lesions in medical images, by using above local segmentation method.

### 5.3. About the parameter settings

The size of local window  $w \times w$  and the coefficient of length term  $\nu$  affect the performance of the proposed model. The value

**Table 3**

The permissible range of length term  $\nu$  used in Fig. 2.

Fig. 2	$[\nu_{\min}, \nu_{\max}]$
a	$[0.020, 0.050] \times 255^2$
b	$[0.015, 0.020] \times 255^2$
c	$[0.010, 0.020] \times 255^2$
d	$[0.010, 0.035] \times 255^2$
e	$[0.005, 0.008] \times 255^2$
f	$[0.100, 0.220] \times 255^2$
g	$[0.150, 0.200] \times 255^2$
h	$[0.450, 0.520] \times 255^2$
i	$[0.100, 0.140] \times 255^2$
j	$[0.080, 0.120] \times 255^2$

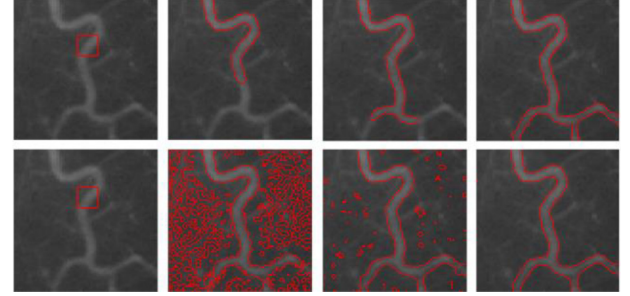


**Fig. 6.** The curve evolution process of the original LIF model and the improved LIF model for a vessel image. Upper row: the original LIF model. Lower row: the improved LIF model.

of  $w$  is similar to the scale parameter  $\sigma$  in the RSF model, which has been proved that it has a strong robustness [16]. For example,  $w=13$  has been used for many images in this paper. For different images, the length term coefficient  $\nu$  needs to be adjusted according to empirical method. For example, in Table 1, we used different value of  $\nu$  to obtain the desired results. But for an image, the suitable  $\nu$  is not unique. Table 3 lists the permissible range of  $\nu$  used in the images in Fig. 2.

### 5.4. Extension of local pre-fitting method

Comparing the RSF energy  $E^{RSF}$  with the proposed energy  $E^{LPF}$ , the only difference is the fitting functions. It means the original fitting functions  $f_1(x)$  and  $f_2(x)$  are replaced by the proposed pre-fitting functions  $f_s(x)$  and  $f_l(x)$ . Because the pre-fitting functions  $f_s(x)$  and  $f_l(x)$  have nothing to do with the level set function  $\phi$ , they do not need to be updated in each iteration. Therefore, using the local pre-fitting functions can improve the segmentation speed and the robustness of initial contour. Similarly, the local pre-fitting method can be easily applied to other local fitting-based active contour models, such as the LIF model and the LGDF model.

Take the LIF model for example, the two fitting functions  $m_1(x)$  and  $m_2(x)$  are totally the same to  $f_1(x)$  and  $f_2(x)$  in the RSF model. Thus, we use  $f_s(x)$  and  $f_l(x)$  to replace  $m_1(x)$  and  $m_2(x)$ , and incorporate the length term  $L(\phi)$  and the distance regularized term  $P(\phi)$ , and keep the others unchanged. Thus, the total energy functional of the improved LIF model is

$$\begin{aligned}
 E^{LIF*}(\phi, f_s, f_l) &= \int_{\Omega} |I(x) - f_s(x)H_\varepsilon(\phi(x)) - f_l(x)[1 - H_\varepsilon(\phi(x))]|^2 dx \\
 &\quad + \nu L(\phi) + \mu P(\phi)
 \end{aligned} \tag{25}$$

Fig. 6 shows the curve evolution process of the original LIF model and the improved LIF model in upper row and lower row, respectively. In the original LIF model, the number of iterations is 240 times and the time spent is 2.122 seconds. But in the

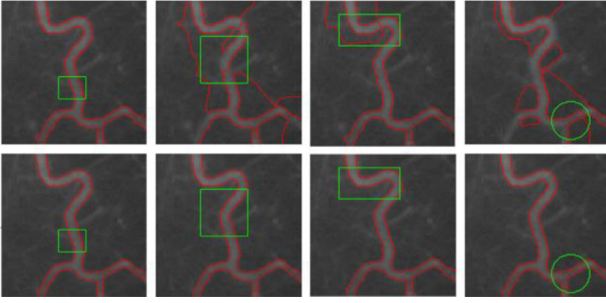


**Fig. 7.** Segmentation results of the original LIF model and the improved LIF model with different initial contours. Upper row: the original LIF model. Lower row: the improved LIF model.

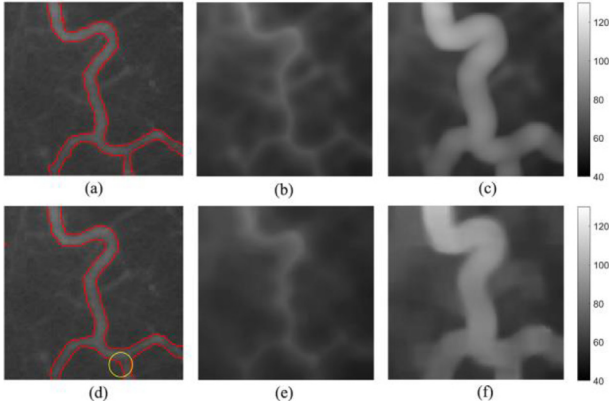


**Fig. 8.** Comparison between the original LIF model and the improved LIF model. (a) Final contour of the original LIF model. (b) The values of  $m_1(x)$ . (c) The values of  $m_2(x)$ . (d) Final contour of the improved LIF model. (e) The values of  $f_1(x)$ . (f) The values of  $f_2(x)$ . (For interpretation of the references to colour in this figure legend, the reader is referred to the web version of this article.)

improved LIF model, the number of iterations is only 18 times and the time spent is 0.081 seconds. It means using local pre-fitting method can reduce the segmentation time obviously. Fig. 7 shows the segmentation results of the original LIF model and the improved LIF model with different initial contours. The results show the improved LIF model is more robust to initial contours than the original LIF model.

In fact, the improved LIF model is the approximation of the original LIF model. Fig. 8 shows the values of  $f_1(x)$  and  $f_2(x)$ ,  $f_s(x)$  and  $f_l(x)$ , and the final contour in the original LIF model and the improved LIF model. From Fig. 8, we can find that the local pre-fitting functions  $f_s(x)$  and  $f_l(x)$  are the approximation of the original fitting functions  $m_1(x)$  and  $m_2(x)$ , respectively. Because of the similarity of the fitting function, the segmentation results of the original LIF model and the improved LIF model are also similar. But the results are not totally same, such as the region circled in yellow line in Fig. 8(d). As a result, using the local pre-fitting method may reduce the segmentation accuracy for some images. In addition, comparing with the original model, the improved model based on local pre-fitting will segment the whole image in general due to the fast emergence of new contours as described in Sections 5.1 and 5.2.

##### 5.5. Application scope of the proposed method

The proposed local pre-fitting model is applicable for the segmentation of two-phase images. But for the images that a part of the object is brighter than the background and other part is darker than the background, such as the image in Fig. 9, it is difficult to segment the objects correctly. For the bright part of object,

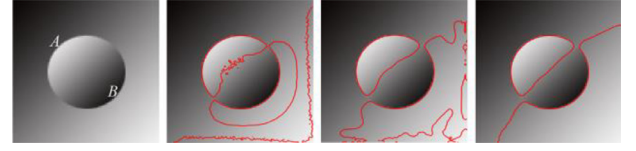


**Fig. 9.** The wrong segmentation results for a synthetic image. Images from left to right represent the process of curve evolution from the initial contour to the final contour.

denoted as the region A in Fig. 9, the curve is evolved inside the boundary. For the dark part of object, denoted as the region B, the curve is evolved outside the boundary. Due to the opposite direction of curve evolution, the segmentation result is wrong. Therefore, the proposed model cannot segment this kind of images.

## 6. Conclusions

In this paper, we have presented an active contour model using local pre-fitting energy, whose advantages are presented below:

1. The proposed model achieves fast segmentation because the computation of local pre-fitting functions is fast and they do not need to be updated in each iteration.
2. The proposed model is robust to initial contours and the initial level set function  $\phi_0$  can be set as a small constant function.
3. The proposed model can be applied for denoising and improving image contrast by using the final fitting image.
4. The proposed local pre-fitting method can be easily applied to other local fitting-based active contour models. Besides the LIF model mentioned in Section 5.4, it can also be used for the LRCV model [19], the LGDF model [20], the LHF model [21], the LLIF model [22] and so on.

Experiments have proved the effectiveness of the proposed model. But it should be noted that the local pre-fitting model proposed in this paper is only applicable for the segmentation of two-phase images.

## References

- [1] N.R. Pal, S.K. Pal, A review on image segmentation techniques, *Pattern Recognition* 26 (1993) 1277–1294.
- [2] D.L. Pham, C. Xu, J.L. Prince, Current methods in medical image segmentation *Annu. Rev. Biomed. Eng.* 2 (2000) 315–337.
- [3] M. Kass, A. Witkin, D. Terzopoulos, Snakes: active contour models, *Int. J. Comput. Vision* 1 (1988) 321–331.
- [4] V. Caselles, F. Catte, T. Coll, F. Dibos, A geometric model for active contours in image processing, *Numer. Math.* 66 (1993) 1–31.
- [5] V. Caselles, R. Kimmel, G. Sapiro, Geodesic active contours, *Int. J. Comput. Vision* 22 (1997) 61–79.
- [6] Y. Zheng, G. Li, X. Sun, X. Zhou, Fast edge integration based active contours for color images, *Comput. Electr. Eng.* 35 (2009) 141–149.
- [7] N. Paragios, R. Deriche, Geodesic active regions and level set methods for supervised texture segmentation, *Int. J. Comput. Vision* 46 (2002) 223–247.
- [8] R. Kimmel, A.M. Bruckstein, Regularized Laplacian zero crossings as optimal edge integrators, *Int. J. Comput. Vision* 53 (2003) 225–243.
- [9] C. Li, C. Xu, C. Gui, M.D. Fox, Distance regularized level set evolution and its application to image segmentation, *IEEE Trans. Image Process.* 19 (2010) 3243–3254.
- [10] C. Xu, J.L. Prince, Snakes, shapes, and gradient vector flow, *IEEE Trans. Image Process.* 7 (1998) 359–369.
- [11] D. Li, W. Li, Q. Liao, Active contours driven by local and global probability distributions, *J. Visual Commun. Image Represent.* 24 (2013) 522–533.
- [12] D. Mumford, J. Shah, Optimal approximation by piecewise smooth function and associated variational problems, *Commun. Pure. Appl. Math.* 42 (1989) 577–685.
- [13] T. Chan, L. Vese, Active contours without edges, *IEEE Trans. Image Process.* 10 (2001) 266–277.
- [14] L. Vese, T. Chan, A multiphase level set framework for image segmentation using the Mumford–Shah model, *Int. J. Comput. Vision* 50 (2002) 271–293.
- [15] A. Tsai, A. Yezzi, A.S. Willsky, Curve evolution implementation of the Mumford–Shah functional for image segmentation denoising, interpolation, and magnification, *IEEE Trans. Image Process.* 10 (2001) 1169–1186.

- [16] C. Li, C. Kao, J. Gore, Z. Ding, Minimization of region-scalable fitting energy for image segmentation, *IEEE Trans. Image Process.* 17 (2008) 1940–1949.
- [17] C. Li, C. Kao, J. Gore, Z. Ding, Implicit active contours driven by local binary fitting energy, in: *Proceedings of the IEEE Conference Computer Vision and Pattern Recognition*, Washington, DC, USA, 2007, pp. 1–7.
- [18] K. Zhang, H. Song, L. Zhang, Active contours driven by local image fitting energy, *Pattern Recognit.* 43 (2010) 1199–1206.
- [19] S. Liu, Y. Peng, A local region-based Chan–Vese model for image segmentation, *Pattern Recognit.* 45 (2012) 2769–2779.
- [20] L. Wang, L. He, A. Mishra, C. Li, Active contours driven by local Gaussian distribution fitting energy, *Signal Process.* 89 (2009) 2435–2447.
- [21] W. Liu, Y. Shang, X. Yang, Active contour model driven by local histogram fitting energy, *Pattern Recognit. Lett.* 34 (2013) 655–662.
- [22] Z. Ji, Y. Xia, Q. Sun, G. Cao, Q. Chen, Active contours driven by local likelihood image fitting energy for image segmentation, *Inf. Sci.* 301 (2015) 285–304.
- [23] Q. Ge, L. Xiao, J. Zhang, Z. Wei, A robust patch-statistical active contour model for image segmentation, *Pattern Recognit. Lett.* 33 (2012) 1549–1557.
- [24] Q. Wu, J. Fang, Parametric kernel-driven active contours for image segmentation, *J. Electron. Imaging* 21 (2012) 043015.
- [25] K. Ding, L. Xiao, G. Weng, Active contours driven by region-scalable fitting and optimized Laplacian of Gaussian energy for image segmentation, *Signal Process.* 134 (2017) 224–233.
- [26] L. Wang, C. Li, Q. Sun, D. Xia, C. Kao, Active contours driven by local and global intensity fitting energy with application to brain MR image segmentation, *Comput. Med. Imaging Graphics* 33 (2009) 520–531.
- [27] C. He, Y. Wang, Q. Chen, Active contours driven by weighted region-scalable fitting energy based on local entropy, *Signal Process.* 92 (2012) 587–600.
- [28] T. Chan, S. Esedoglu, M. Nikolova, Algorithms for finding global minimizers of image segmentation and denoising models, *SIAM J. Appl. Math.* 66 (2006) 1632–1648.
- [29] Y. Yang, C. Li, C.Y. Kao, S. Osher, Split Bregman method for minimization of region-scalable fitting energy for image segmentation, in: *Proceedings of the International Symposium on Visual Computing*, Las Vegas, Nv, USA, 2010, pp. 117–128.